Science and Technology Indonesia
e-ISSN:2580-4391 *p*-ISSN:2580-4405
Vol. 8, No. 4, October 2023

Research Paper

A Study of the Magnetic Properties and Structure of Heusler Alloys Prepared by Arc-Melting Technique

N. A. Khalefa[1*]

[1]*Medical Instruments Techniques Engineering Department, Al-maarif University College, 31001, Iraq*
***Corresponding author**: najm.abdullah@uoa.edu.iq

Abstract
Heusler alloys were prepared in this study using the Arc-Melting method in which 30 g of the Arc-melting pure elements were combusted in an Argon arc furnace. Saturation magnetization, X-ray diffraction (XRD) analysis, and scanning electron microscope (SEM) were used to characterize the prepared alloys in terms of the compositions (Co_2TiZ), where Z= Al, Ge, Sb are related IVB sub-group metals. In this work, the specimens containing Ge and Ti have fully Ferro magnetically order and $L2_1$ chemical structure with magnetism due to the magnetic moments attributed to the Co site. The Heusler alloys containing IIB or IVB sub-group metals such as Al, Ti, or Ge behave ferromagnetism, with the magnetic moments being attributed to the magnetic moments of the Co sites. Heusler alloys containing the group IVB element such as Sb exhibited vacant chemical effects with Co sites, and they also contain some paramagnetic compounds. Heusler alloys with Sb element exhibited paramagnetic behavior with vacant chemical order. Alloys demonstrate different magnetic properties as a result of temperature change and exchange interaction with atomic structure.

Keywords
Heusler Alloys, Co_2MnZ, Ferromagnetic, Arc-melting, Paramagnetic Susceptibilities

Received: 1 July 2023, Accepted: 18 October 2023
https://doi.org/10.26554/sti.2023.8.4.36-42

1. INTRODUCTION

Heusler alloys with a half-filled d-electron shell are ternary intermetallic magnetic compounds in the order CoTiZ, where Z represents sub-group metals. The crystal structure of $L2_1$-type alloys is shown in Figure 1. Recently, new samples of such materials, as used in this research, have exhibited both superconductivity behavior and magnetism. The effect of inter-atomic distances, electron concentration, and atomic arrangement on the magnetic properties of some alloys is studied using the vibrating sample magnetometer (VSM). The magnetic properties and principle magnetic features (particle size) of Heusler alloys are listed in Table 1.

Studies on the properties of Heusler alloys that contain transition elements have recently increased significantly as a result of the availability of pure materials and a wealth of physical phenomena in pure metals, as well as in their compounds. The rare-earth elements are characterized by having a partially filled f-electron shell that consists of either 3d or 4d-electrons (Bachagha and Suñol, 2023; Marathe and Herper, 2023).

Apart from the particular behavior of a half-filled level d-electron shell, the unfilled d-electron shell will produce a magnetic moment. The exchange of the interaction between d-electron magnetic moments causes a variety of exchange of magnetic phenomena in the rare earth and transitions metals and their compounds. In addition to the magnetic phenomena, an interaction occurs between the degrees of freedom and the lattice constant of freedom which leads to the lattice phenomenon (Rogl and Rogl, 2023).

Despite the considerable progress in understanding the basic interactions in these materials, there is still uncertainty in some cases regarding the mechanism responsible for the observed phenomena. In addition to the properties in Heusler alloys observed such as very weak behaviour ferromagnetism phase occurs exchange, they enhance Pauli Para magnetism. In the Pd_2MnIn Hamri (2016) compound, anti-ferromagnetism is a consequence of the exchange of orbital interaction between the atoms that have been found arranged either in layers or chains, and those provide a useful illustration. As a result of the fully-order in the $L2_1$ structure, the expected super lattice line intensities of the pattern are only of the order of 2 percent of the line intensity of the principal reflections (Tavares et al., 2023).

The crystal structures of $L2_1$ and B_2 types Co_2TiZ (Z= Al, Ge, Sb) are presented in Figure 1. Heusler alloys have been given two Co atoms sitting at equivalent sites and Co_1, Co_2, Ti, and Z atoms occupy the Wyckoff coordinates (Zawar et al.,

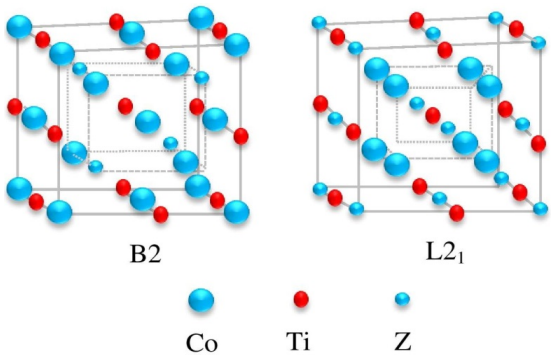

Figure 1. The Crystal Structure of the $L2_1$ and B2 Types for Co_2TiZ (Z= Al, Ge, and Sb Heusler Alloys)

2019). In the rare earth metals, the 3d have filled electrons that exhibit the magnetic properties of the Heusler alloys as a result of their magnetic moment found in a subsite with local symmetry for unit cell, such as in Pd_2(Re)Sn, where (Re) represents heavy rare elements such as Tb and Lu; this sample also exhibits a strong magneto-crystalline anisotropy behavior (Zhou et al., 2006; Jin and Jung, 2022).

As a result of a large orbital shell contribution to the Cobalt element, magnetic moment appears as an unusual result of magnetization of the Heusler alloy which is dominated by the Co atoms, and the second order is induced for anisotropy term constant. Therefore, the value of the magnetization depends on the relative value importance of the local anisotropy of the (Re)-Co exchange interaction; the onset of 3D magnetization is from the magnetism of the free itinerant electrons. At a high Curie temperature (≈ 1000k) and room temperature, large spontaneous magnetization and uniaxial anisotropy occur in three compounds which makes them suitable for many magnetic applications (Hu et al., 2020).

The magnetic properties and chemical structure of Heusler alloys mainly depend on the method of specimen preparation (Lee et al., 2015). Heusler alloys are commonly produced using high-temperature solid-state reactions between the constituents of the transition elements (X); Y is either Mn or (Z) as a B subgroup metal (Chen et al., 2006). Investigation of the magnetic properties of Pd_2MnZ, Au_2MnZ, and Co_2MnZ has shown that all the samples have crystalline structures with magnetic moments value of approximately 4μB on the Mn site.

Most of the Heusler alloys exhibit a ferromagnetic phase, but some of them behave as anti-ferromagnetic (AF) structures that have been found recently (Galanakis et al., 2002; Sanvito et al., 2017). For example, the Co_2MnZ compound (Galanakis et al., 2002) exhibits a magnetic moment on the Mn sites, and in addition to that, has a substantial magnetic moment caused by the cobalt (Co) sites (Sanvito et al., 2017). These results cause an increase in the value of the exchange interaction and the corresponding higher Curie temperature (Tc) (Ruban et al., 2007).

In the present work, there are small differences between the values of the atomic specific scattering factor for Co element and Ti; the absorption correction only provides a qualitative indication of the type of the chemical order according to the X-ray results, with neutrons scattering, and absorption corrections which usually indicate small and essentially isotropic. By employing neutron scattering, the result shows that the magnitude and sign of the scattering length for Co and Ti atoms are different. This normally shows the quantitative description of the chemical order structure of the alloys to be made; this behavior is supported by the X-ray diffraction pattern epically used in C_{lb}-type compounds, such as Co_2TiSb. The problem of structure ordering in such samples is essential to prove the quaternary of Heusler alloy which has three types from rare earth atoms and one vacancy order on the four occupation sites. This work is an effort to understand the magnetic behavior of Heusler alloy in light of the differences in the reported experimental results. The apparent sensitivity of the paramagnetic phases depends on the method of sample preparation and measurement. In this work, three Heusler alloy samples were prepared using the arc melting method; the investigation of their structure and magnetic properties was done using X-ray diffraction and scanning electron microscopy (Pullar, 2012).

2. EXPERIMENTAL SECTION

2.1 Materials

Heusler alloy were prepare during this work such as Co_2TiAl, Co_2TiGe, and Co_2TiSb The starting element for this study was supplied by Johson Matthey Chemicals Ltd, the details of which are given (Khalefaa, 2019). For the magnetic investigation, the samples were rough and ellipsoids with a diameter of 3.5 mm and length of 1.5 mm. The surface of the samples was chemically polished to remove surface contaminants.

2.2 Methods

The structure of all the alloys in this study was determined using the XRD technique at room temperature. A Philips diffractometer with a broad focus tube Pw 2013/100 with copper target was used for the XRD analysis (λ= 0.154 A). The observed position of the Bragg pattern for the peaks of each line and the lattice parameter were used to measure the accurate value of the sub-lattice strain and the grain size using the Philips (APD 372) based on the XRD results. The line profiles software that accompanies the Philips was used during the X-ray diffracting line broadening analysis for the calculation of the grain size; the strain parameters for the Heusler alloys were measured by analyzing either the (111) peak or the (200) peak for Co_2TiAl, Co_2TiGe, and Co_2TiSb alloys, and this is dependent on their crystal structures (Hu et al., 2020).

A scanning electron microscope (SEM) was used to investigate the surface morphologies of the alloys and the particle size distribution for the prepared samples. The SEM images show that the samples are composed of uniformly distributed near-spherical particles with diameters ranging from 31 – 60 emu (see Table 1). The particle distribution appears to be similar for the alloys (Co_2TiAl and (Co_2TiGe) and finer for the

alloy Co_2TiSb. The size magnetic analysis showed that all the alloys were ferromagnetic except Co_2TiSb. A Foner vibration sample of the magnetometer (VSM) was used to measure the bulk magnetization of the samples. The magnetic properties were calculated in an applied field of up to 16 Koe at different temperature ranges (4.2 – 400 K) (Ma et al., 2011).

2.3 Characterization

All the samples were prepared in an essentially similar method using the Arc-melting method which was considered to be the most suitable for the preparation of Heusler alloys; it is also a good method for the study of the magnetic properties of such alloys, such as spectrographic and surface morphology studies, as well as their susceptibilities with temperature variation (Heczko et al., 2022).

The corrections of the demagnetization were measured to annul the thermal diffuse scattering effect. Also, the spontaneous magnetization $\sigma 0$s was calculated from the extrapolation of $\sigma 2$ vs H/σ plots (Welzmiller et al., 2013). The spontaneous magnetization (σs) curves to 0 K were measured based on the $\tau 3/2$ law to estimate the saturation magnetization (Ms). Furthermore, paramagnetic susceptibilities with temperature variation were measured using the Smith ring balance calibrated against pure Pd (Graf et al., 2011; Vinogradov et al., 2005). The saturation magnetization measurements (Ms) for each Heusler alloy were done using a high-field hysteresis loop technique (Chauhan et al., 2004). The low field Ac magnetic susceptibility (χ), as a function of temperature measurements for powder specimens, was carried out in the temperature range of 300-800K using the double coil set-up (Berenson et al., 1984).

3. RESULTS AND DISCUSSION

The X-ray diffraction (XRD) spectra revealed that some of the specimens were chemically disordered at the B2 structure which is an interesting observation in this work. The other samples have an $L2_1$ structure and this behavior, which is a result of the atomic order of the specimens, gives rise to the occurrence of magnetism and superconductivity. Figure 2 shows the hkl value of each peak and the representative XRD pattern. The lattice constant of the specimens resulted from the X-ray diffraction data analysis with an accuracy of ± 0.00 2A.

The magnetic properties were measured at room temperature (RT) using the pules field hysteresis loop tracer technique. The saturation magnetization (Ms) Coercivity (Hc) and reminisce magnetization (Mr) were obtained using the M-H plot (Figure 3). The M-H loop at 300k exhibits superparamagnetic behavior of the samples. From the hysteresis curve of the ferromagnetic state, the values of Hc, Mr, and Ms were deduced and given in Table 2. The hysteresis loop calculation shows that the magnetization curve is shifted vertically and horizontally, where the horizontal shift of the hysteresis loop is larger and indicates the magnetic field flex effect. Furthermore, at finite temperatures, there is a strong thermal dependence as

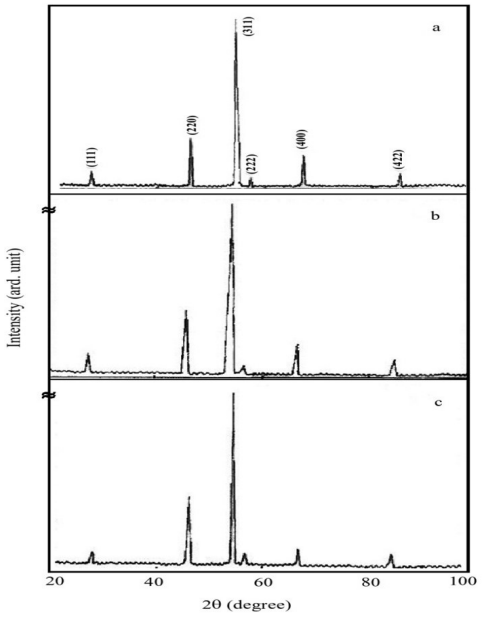

Figure 2. Typical X-ray Diffraction Pattern: a) for Co_2TiAl, b) for Co_2TiGe, and c) for Co_2TiSb

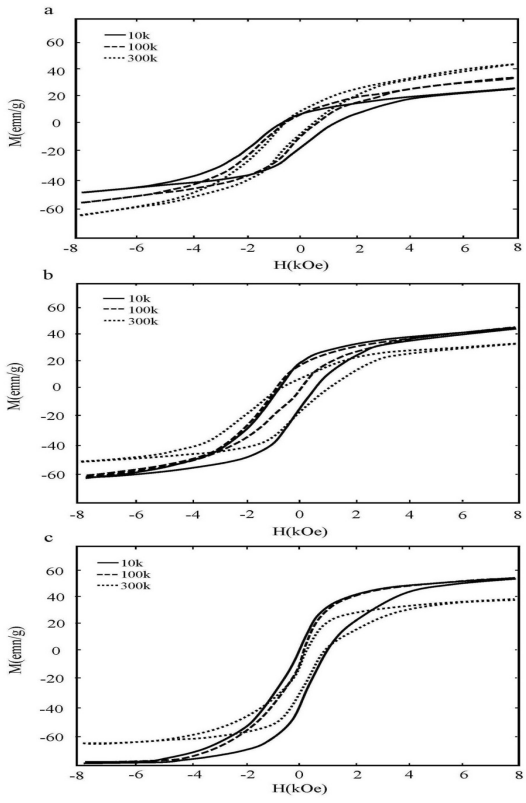

Figure 3. M-H Loop for Some Heusler Alloys Annealing at 300 K for 2 h: a) Hysteresis Loop for Co_2TiAl, b) Hysteresis Loop for Co_2TiGe, and c) Hysteresis Loop for Co_2TiSb

Table 1. Lattice Parameters, X-Ray Pattern, and the Particle Size of Co_2TiAl, Co_2TiGe, and Co_2TiSb

Alloy	Curie Temp. (K)	$\sigma 00$ (e.m.ug^{-1})	$\mu 00$/mol	Lattice Constant (A°)	Particle Size (emu)
Co_2TiAl	215 ± 3	67.7 ± 0.6	0.71 ± 0.003	5.396	31
Co_2TiSb	289 ± 4	60.28 ± 1.0	1.93 ± 0.07	5.081	25
Co_2TiGe	365 ± 4	71.5 ± 1.0	0.75 ± 0.003	5.17	60

Table 2. The Magnetic Data in the Temperature Range of 10 to 300 K. Measurements Obtained using VSM Experimental Values of the Saturation Magnetization Showed that Ms was Achieved by the Applied Magnetic Field

Alloy	Temperature	Saturation Magnetization (Ms) emu/g	Remnant (Mr)	Coercivity (Hc)	SQR (Mr/Ms)	Structure	hkl
	10	87.688	11.560	540.06	0.13183		(111)
Co_2TiAl	100	81.675	12.347	604.67	0.15108	B2	(200)
	300	65.337	13.321	860.57	0.1767		(220)
	10	77.921	20.925	785.60	0.286		(111)
Co_2TiGe	100	74.475	17.550	615.15	0.2356	$L2_1$	(200)
	300	64.335	17.556	612.68	0.2919		(311)
	10	86.597	22.282	573.94	0.2574		(111)
Co_2TiSd	100	86.271	14.811	432.40	0.1718	$L2_1$	(200)
	300	67.016	9.224	378.27	0.1313		(222)

the field flex at T= 300 K is less than a quarter of the value at T= 10 K. This also agrees with the coercivity (Hc) small flex measurement at low temperatures (see Figure 3).

There is a change in MH-loop behavior with temperature as shown in Figure 3 due to the change in short-range order. This change is probably due to atomic rearrangement, such as short-range ordering, and clustering or spindle decomposition. According to experimental values, the saturation magnetization (Ms) versus temperature plot shows that the lower temperatures produced higher saturation magnetization values in each specimen. The reminisce magnitude records an increase with temperature (from 11.5 emu/g at 100 K to 14.63 emu/g at 300 K). The SQR (Mr/Ms) was obtained by measuring the squareness of the hysteresis curve. In this research, the samples recorded increases in SQR (Mr/Ms) as a function of the temperature range (from 0.131 at 100 K to 2.242 at 300 K). Although the temperature range was more restricted in the present research, the variation of magnetic susceptibility is small (Cugini et al., 2022); hence, the susceptibility analysis was conducted using the following Equation 1:

$$X(T) = X(O) + CT \quad (1)$$

At high temperatures, i.e., T > 150 K, the data was compared to the expression of Equation 2 using least squares analysis. The purpose of using the high-temperature region was to avoid the problems due to short-range order arrangement; however, the agreement shown in Figure 4 is convincingly due to low temperature. Furthermore, the demagnetization contribution expression was measured using Equation 2.

$$X^{mol} = -Zi\frac{Ne^2}{6mc^2}\langle r^2\rangle \quad (2)$$

Where Zi represents the number of 3d-electrons shell in the atom; $\langle r^2\rangle$ is the average value of the square radius of the 3d-electron.

The paramagnetic contribution of the sample material is just an additive term of the components, and is given in Equation 3:

$$X^{dem}\ (M_mX_n = M_x{}^{dem}(m) + n\ X^{dem}\ (X) \quad (3)$$

The table of the values of the terms in Equation 3 may be found in the literature (Kotliar et al., 2006).

Table 2 summarizes the data for all the samples; the Coercivity (Hc) numerical results were observed to generally agree with those published in the literature (Graf et al., 2011; Ma et al., 2011). The obtained results show increasing Coercivity as a result of the increase in temperature (between 10 to 300 K).

The observation indicates an isotropic peak which could be seen in magnetic materials with a multi-domain state. The relationship between the susceptibility χAc (T) and the coercive force (Hc) is inversely proportional; therefore, increases in the As susceptibility only appeared after the second peak due to a decline in the value of the coercive force. The existence of

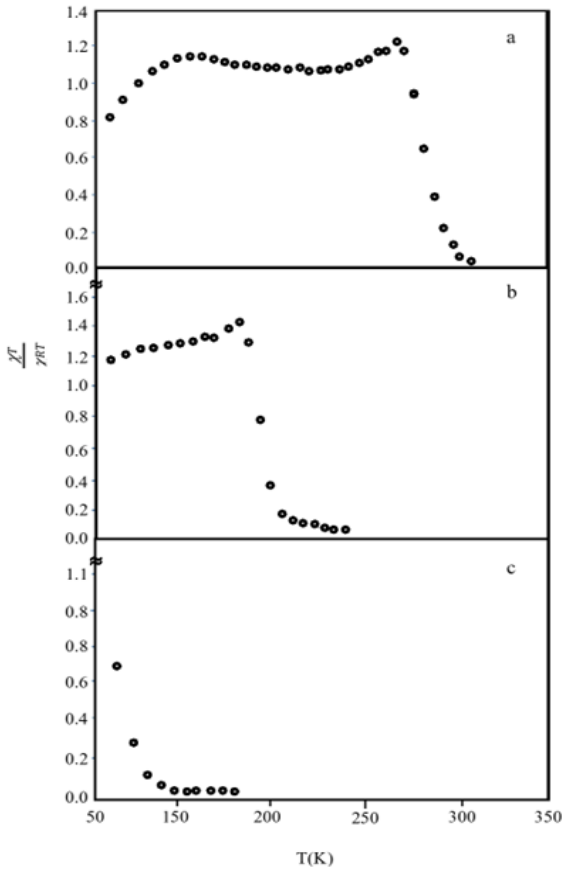

Figure 4. The Variations in Susceptibility with Temperature: a) for Co_2TiAl, b) for Co_2TiSb, c) for Co_2TiGe

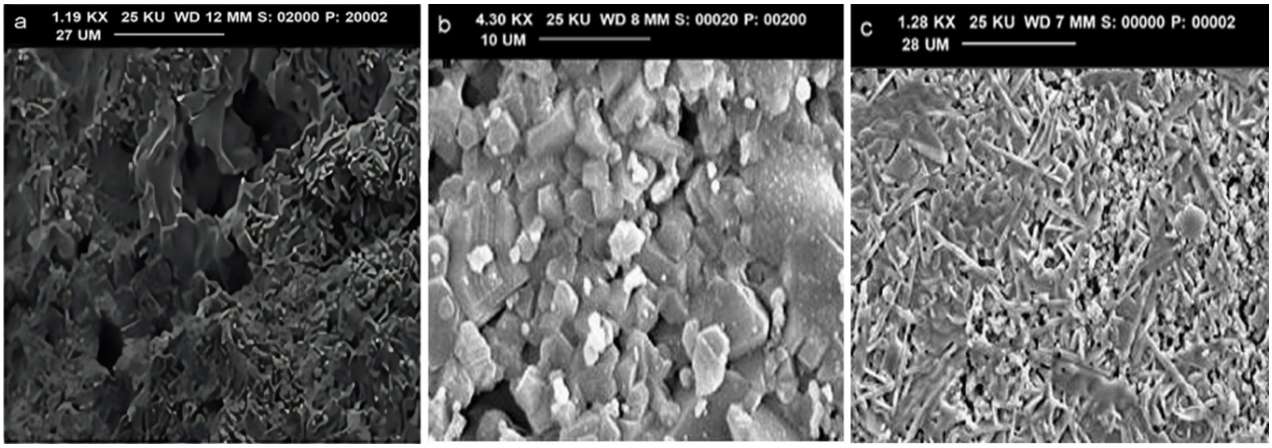

Figure 5. Scanning Electron Microscope (SEM): a) for Co_2TiAl, b) for Co_2TiGe, and c) for Co_2TiSb

the coercive force indicates that the specimens contain clusters shape of different sizes and each spin arrangement in the cluster should be large because of a large blocking temperature for samples (Zhang et al., 2022). The Curie temperature (Tc) determined in Figure 4 is given in Table 1.

Figure 5 presents the SEM image, the cross-section, and the free surface morphology and microstructure of the three alloys (Co_2TiAl, Co_2TiGe, and Co_2TiSb) at different magnifications. The figure showed a nearly equated grain shape similar to the grain shape reported by Pullar (2012).

4. CONCLUSION

Arc-melting method proved to be suitable for the preparation of Heusler alloys in this work; it plays an important role in

controlling the magnetic properties of the alloys. The simultaneous substation of transition elements (Al, Sd) has a strong influence on their magnetic and structural properties. The lattice constant obtained from the X-ray data in this work showed a non-linear behavior. The observed and calculated susceptibility values for each alloy suggest the existence of obvious canting at the octahedral B sites.

5. ACKNOWLEDGEMENT

The author is grateful for the support from Al-maarif University College.

REFERENCES

Bachagha, T. and J. Suñol (2023). All-d-Metal Heusler Alloys: A Review. *Metals*, **13**(1); 111

Berenson, G. S., B. Radhakrishnamurthy, S. R. Srinivasan, P. Vijayagopal, E. R. Dalferes Jr, and C. Sharma (1984). Recent Advances in Molecular Pathology: Carbohydrate—Protein Macromolecules and Arterial Wall Integrity—A Role in Atherogenesis. *Experimental and Molecular Pathology*, **41**(2); 267–287

Chauhan, B., R. Kumar, K. Jadhav, and M. Singh (2004). Magnetic Study of Substituted Mg–Mn Ferrites Synthesized by Citrate Precursor Method. *Journal of Magnetism and Magnetic Materials*, **283**(1); 71–81

Chen, X., R. Podloucky, and P. Rogl (2006). *Ab Initio* Prediction of Half-Metallic Properties for the Ferromagnetic Heusler Alloys CO_2 *M* Si (*M* = Ti, V, Cr). *Journal of Applied Physics*, **100**(11)

Cugini, F., S. Chicco, F. Orlandi, G. Allodi, P. Bonfá, V. Vezzoni, O. Miroshkina, M. Gruner, L. Righi, S. Fabbrici, et al. (2022). Effective Decoupling of Ferromagnetic Sublattices by Frustration in Heusler Alloys. *Physical Review B*, **105**(17); 174434

Galanakis, I., P. Dederichs, and N. Papanikolaou (2002). Slater-Pauling Behavior and Origin of the Half-Metallicity of the Full-Heusler Alloys. *Physical Review B*, **66**(17); 174429

Graf, T., C. Felser, and S. S. Parkin (2011). Simple Rules for the Understanding of Heusler Compounds. *Progress in Solid State Chemistry*, **39**(1); 1–50

Hamri, B. (2016). *Investigation Théorique Des Propriétés Structurales, électroniques Et Magnétiques Des Alliages Heusler Ti2VZ (Z = Ge, Sn, Pb)*. Ph.D. thesis

Heczko, O., H. Seiner, and S. Fähler (2022). Coupling between Ferromagnetic and Ferroelastic Transitions and Ordering in Heusler Alloys Produces New Multifunctionality. *MRS Bulletin*, **47**(6); 618–627

Hu, J., S. Granville, and H. Yu (2020). Spin-Dependent Thermoelectric Transport in Cobalt-Based Heusler Alloys. *Annalen Der Physik*, **532**(11); 1900456

Jin, T. and Y. Jung (2022). Recent Progress in Computational Discovery of Heusler Alloys. *Bulletin of the Korean Chemical Society*, **43**(4); 484–491

Khalefaa, N. (2019). Effect of Annealing Treatment Processes on Structural and Magnetic Properties for Some Invar Alloys. *International Journal of Engineering Research and Technology*, **12**(1); 102–106

Kotliar, G., S. Y. Savrasov, K. Haule, V. S. Oudovenko, O. Parcollet, and C. Marianetti (2006). Electronic Structure Calculations with Dynamical Mean-Field Theory. *Reviews of Modern Physics*, **78**(3); 865

Lee, N., D. Yoo, D. Ling, M. H. Cho, T. Hyeon, and J. Cheon (2015). Iron Oxide Based Nanoparticles for Multimodal Imaging and Magnetoresponsive Therapy. *Chemical Reviews*, **115**(19); 10637–10689

Ma, L., W. Wang, J. Lu, J. Li, C. Zhen, D. Hou, and G. Wu (2011). Coexistence of Reentrant-Spin-Glass and Ferromagnetic Martensitic Phases in the $Mn_2Ni_{1.6}Sn_{0.4}$ Heusler Alloy. *Applied Physics Letters*, **99**(18)

Marathe, M. and H. C. Herper (2023). Exploration of All-3 *d* Heusler Alloys for Permanent Magnets: An *ab Initio* Based High-Throughput Study. *Physical Review B*, **107**(17); 174402

Pullar, R. C. (2012). Hexagonal Ferrites: A Review of the Synthesis, Properties and Applications of Hexaferrite Ceramics. *Progress in Materials Science*, **57**(7); 1191–1334

Rogl, G. and P. F. Rogl (2023). Development of Thermoelectric Half-Heusler Alloys over the Past 25 Years. *Crystals*, **13**(7); 1152

Ruban, A. V., S. Khmelevskyi, P. Mohn, and B. Johansson (2007). Magnetic State, Magnetovolume Effects, and Atomic Order in Fe_{65} Ni_{35} Invar Alloy: A First Principles Study. *Physical Review B*, **76**(1); 014420

Sanvito, S., C. Oses, J. Xue, A. Tiwari, M. Zic, T. Archer, P. Tozman, M. Venkatesan, M. Coey, and S. Curtarolo (2017). Accelerated Discovery of New Magnets in the Heusler Alloy Family. *Science advances*, **3**(4); e1602241

Tavares, S., K. Yang, and M. A. Meyers (2023). Heusler Alloys: Past, Properties, New Alloys, and Prospects. *Progress in Materials Science*, **132**; 101017

Vinogradov, A., T. Ishida, K. Kitagawa, and V. Kopylov (2005). Effect of Strain Path on Structure and Mechanical Behavior of Ultra-Fine Grain Cu–Cr Alloy Produced by Equal-Channel Angular Pressing. *Acta Materialia*, **53**(8); 2181–2192

Welzmiller, S., P. Urban, F. Fahrnbauer, L. Erra, and O. Oeckler (2013). Determination of the Distribution of Elements with Similar Electron Counts: A Practical Guide for Resonant X-Ray Scattering. *Journal of Applied Crystallography*, **46**(3); 769–778

Zawar, S., S. Atiq, M. Tabasum, S. Riaz, and S. Naseem (2019). Highly Stable Dielectric Frequency Response of Chemically Synthesized Mn-Substituted $ZnFe_2O_4$. *Journal of Saudi Chemical Society*, **23**(4); 417–426

Zhang, Q., M. Qian, and X. Zhang (2022). Magneto-Structural Transition and Refrigeration Property in All-D-Metal Heusler Alloys: A Critical Review. *Journal of Solar Energy Research Updates*, **9**; 52–69

Zhou, X., H. Kunkel, G. Williams, S. Zhang, and X. Desheng

(2006). Phase Transitions and the Magnetocaloric Effect in Mn Rich Ni–Mn–Ga Heusler Alloys. *Journal of Magnetism and Magnetic Materials*, **305**(2); 372–376